Silicon Nitride-Based Compact Double-Ring Resonator Comb Filter With Flat-Top Response

J. F. Song, Q. Fang, S. H. Tao, M. B. Yu, G. Q. Lo, and D. L. Kwong

***Abstract*—A novel double-ring resonator comb filter structure with flat-top response is proposed and fabricated. In this letter, we discuss its function theoretically and present results from devices fabricated on silicon nitride. The measured results show a flat-top response profile for the transverse-magnetic mode over C- and L-band, with the channel isolation $\sim$15 dB, the free spectral range $\sim$3 nm, and the total insertion loss ~ -7.5 dB. The footprint of the device is $\sim 450\ \mu\text{m} \times 250\ \mu\text{m}$.**

***Index Terms*—Comb filters, integrated optics, resonator filters.**

I. Introduction

RECENTLY, Si-based microphotonics has received growing interests in research and development of new-generation high-speed high-volume communication and computation devices. Optical components with high-performance and ultracompact size with leveraging on existing Si complementary metal–oxide–semiconductor infrastructure are highly demanded for realizing the large-scale photonic-integrated circuits. Optical comb filters, making use of the constructive and destructive light interferences to create regularly spaced multichannels, are key devices in a wavelength-division-multiplexer system. A comb filter requires periodic and flat-top response. Many comb filters, such as fiber-based [1], [2], Sagnac birefringence based [3], Michelson–Gires–Tournois [4], and Mach–Zehnder interferometers (MZIs) [5]–[8], have been reported. Generally, fiber-based comb filters must work with other elements. Furthermore, adopting a cascade MZI structure increases the length of the device. Planar lightwave circuit comb filters have drawn more attention recently because they can be integrated with other functional devices on a single chip. Wu *et al.* [7] fabricated a nested MZI structure on polymer, where an MZI structure nested with one another. The obtained channel isolation was $\sim$22 dB. Bidnyk *et al.* [8] also used elliptical grating facets to construct a comb filter.

It is known that a ring-resonator (R-R) add–drop system can have periodic spectrum response. Such a structure with an MZI has been applied as optical interleaver [9]–[11]. However, the response spectrum of an interleaver is limited to odd or even number of channels whereas a comb filter is required to have full-channel response, and the R-R system itself can be a choice for comb filters, especially with a high self-coupling coefficient. But the output sideband roll-off will be too narrow. On the contrary, if the self-coupling coefficient is decreased, the output sideband roll-off becomes wider and lighter power will be coupled to the drop port.

In this letter, we propose a compact double-ring resonator coupling system which functions as a comb filter. First, we describe the operation principle theoretically. Then we present the performance of the fabricated structure on silicon nitride (SiN). The device is with compact footprint.

Manuscript received April 23, 2008; revised September 16, 2008. First published October 31, 2008; current version published December 12, 2008.

J. F. Song is the Institute of Microelectronics, A*STAR, Singapore 117685, Singapore, and also with State Key Laboratory on Integrated Opto-Electronics, College of Electronic Science and Engineering, Jilin University, Changchun 130023 China (e-mail: songjf@ime.a-star.edu.sg).

Q. Fang, S. H. Tao, M. B. Yu, G. Q. Lo, and D. L. Kwong are with the Institute of Microelectronics, A*STAR, Singapore 117685, Singapore.

Color versions of one or more of the figures in this letter are available online at http://ieeexplore.ieee.org.

Digital Object Identifier 10.1109/LPT.2008.2006992

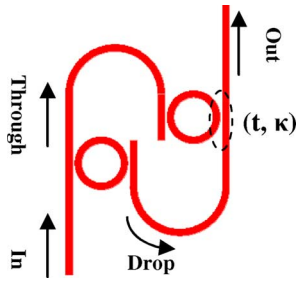

Fig. 1. Schematic of the double-ring resonator comb filter structure.

II. Operation Principle

The proposed structure is shown in Fig. 1. It consists of two R-Rs. The incident light is split into two beams, through and drop. In this structure, the drop waveguide of the first R-R acts as the through-waveguide of the second R-R. There are four coupling points between the waveguides and the R-Rs (denoted in Fig. 1 by dashed ellipse). The coupling points have the same self- and cross-coupling coefficients. For a single R-R, as we know, the through- and drop-lights can be described by (1). The output transfer function of the full device is $H^{(\text{out})} = 2H^{(\text{through})} \cdot H^{(\text{drop})}$

$$\begin{cases} H^{(\text{through})} = \frac{E^{(\text{through})}}{E^{(\text{input})}} = \frac{t[\gamma \exp(i\theta) - 1]}{t^2 \gamma \exp(i\theta) - 1} \\ H^{(\text{drop})} = \frac{E^{(\text{drop})}}{E^{(\text{input})}} = \frac{\sqrt{\gamma} \exp\left(i\frac{\theta}{2}\right)\kappa^2}{t^2 \gamma \exp(i\theta) - 1} \end{cases} \tag{1}$$

where H denotes the transfer function, which is a ratio between the input and the output wave functions. θ is the total phase shift for light that runs one round in the ring and can be described as: $\theta = n_r L_c k_0 = n_r L_c \omega / c$. Since θ is a function of frequency ω, we will not distinguish θ and ω in the following discussion. L_c is the perimeter of the ring, k_0 is the wave number in vacuum, and c is the velocity of light in vacuum. We define the amplitude

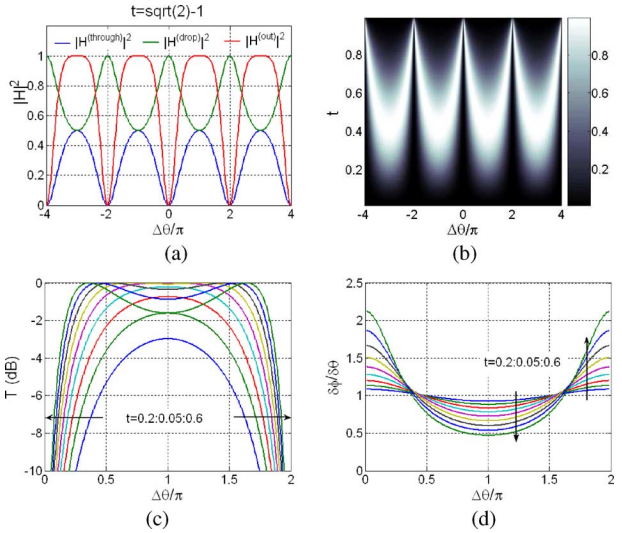

Fig. 2. (a) Transmission spectra of through (blue), drop (green), and output (red). (b) Transmission spectra with varying t. (c) Expanded view of (b). t increased from 0.2 to 0.6 with step 0.05. (d) Related time delays corresponding to (c). Arrows show the trends of increasing t in (c) and (d).

loss coefficient as $\gamma = \exp(-n_i L_c k_0)$. In the following analysis, we assume there is no loss ($\gamma = 1$), $t^2 + \kappa^2 = 1$, where n_r and n_i are the real and imaginary parts of the effective refractive index, respectively. As an example of $t = \sqrt{2} - 1$, the through- and drop-light transmission spectra are shown as blue and green curves in Fig. 2(a). They are periodic (2π), oscillatory, and complementary functions of frequency. The output light is shown as red line in Fig. 2(a). It shows flat-top response. The -1-dB passband width is $\sim$51% of the channel spacing.

In this structure, ring radius determines the width of free spectral range (FSR), which is related to the wavelength width of $\Delta\theta = 2\pi$. The coupling coefficients determine the profile of the spectrum response. Fig. 2(b) shows the transmission spectra of $|H^{(\text{out})}|^2$ as a function of self-coupling coefficient t. When t is near zero, there is no light coming out of the output waveguide. When t is near one, the transmission spectra present double narrow peaks, and the valleys between two peaks are at the points of $\Delta\theta$ in π multiple. When t is near $\sqrt{2} - 1$, the spectrum shows a flat-top and box-like profile. Fig. 2(c) shows the details with t increasing from 0.2 to 0.6 with step of 0.05. From (1), we can obtain maximum flat-top situation as t is equal to $\sqrt{2} - 1$;[1] if t is less than $\sqrt{2} - 1$, the spectrum displays protuberant, and if t is greater than $\sqrt{2} - 1$, the spectrum is concave.

The group delay time is defined as negative differential of phase to angle frequency

$$\tau = -\frac{\partial \varphi}{\partial \omega} = -T_c \frac{\partial \varphi}{\partial \theta} \tag{2}$$

where T_c is the time of light running a full round in a ring, and φ is the phase of the output light. The curves in Fig. 2(d) represent the corresponding related time delays. For a small t, the delay time shows flatter profile in the spectrum. But with increasing t, the passband has a shorter delay than the stopband.

[1]Because flat-top is near $\theta = \pi$, we set $\theta = \pi + \Delta\theta$; from (1), we can get $|H^{(\text{out})}|^2 = 1/[1 + (\Delta\theta)^4/64]$, when $1 - t^2 = 2t$, or $t = \sqrt{2} - 1$. It is just as a second-order Butterworth filter with maximum flat-top modality.

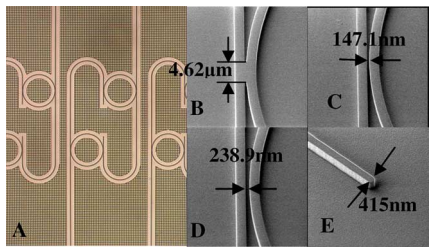

Fig. 3. (A) microscope picture of the devices. (B)–(E) are SEM pictures. (B) shows connected waveguides. (C) and (D) display varying gaps. (E) is an SSC. The tip width of the SSC is 415 nm, and the length is 200 μm.

III. Fabrication and Measurement

Starting with an 8-in bulk Si-substrate, we first deposited a 5-μm low-stress silicon dioxide ($SiO_2 \sim 1.45$) bottom layer. To reduce the SiO_2 surface roughness, we employed chemical mechanical polishing. Subsequently, SiN ($\sim$2.33), as the core waveguide layer, was deposited on top of the SiO_2 layer by plasma-enhanced chemical vapor deposition. The 248-nm-deep ultraviolet lithography was used for the waveguide patterning process. Waveguide etch was processed by reactive ion etching followed by photoresist removal and polymer wet clean. Finally, 4-μm SiO_2 was deposited over the structures as the top cladding layer. In this fabrication, the ring resonator comb filter with a waveguide width of 825.7 nm, waveguide thickness of 400 nm, radius of 60 μm, and device footprint of $\sim 450\ \mu\text{m} \times 250\ \mu\text{m}$ was achieved.

A top-down microscope picture of the device is presented in Fig. 3(a). For this structure, a key parameter is self-coefficient t, which is sensitive to the spacing between the waveguide and the ring. Thus, we can control t by varying the gap spacing. Three gaps with varying spacing had been fabricated. The scanning electron microscope (SEM) pictures of these gaps are shown in Fig. 3(B), (C), and (D), respectively. Fig. 3(B) is the situation that the ring connects with the waveguide. The length of the connected region is $\sim$4.62 μm. The gap spacing in (C) and (D) are 147.1 and 238.9 nm, respectively. Since the light is transferred from the input waveguide to the coupled waveguide by crossing the coupling region, a wider gap will transfer less light. For coupling the input and output of the light efficiently, spot size converters (SSCs) had been integrated in the input and output of the waveguides, respectively. The width of the SSC in Fig. 3(E) is $\sim$415 nm, and the length is 200 μm.

During measurement, the insertion loss (IL) was recorded as the fiber to fiber loss, which included the device transmission loss and the coupling loss between a fiber and an SSC. Two lensed polarization-maintaining fibers (LPMFs) were used to couple light with the input and output waveguides, respectively. The focus spot size of the LPMF was $\sim$2.5 μm. For the waveguide, we used the cutback method to investigate polarization-dependent loss (PDL) (EXFO IQS-12004B). Moreover, we used a polarization controller to choose a quasi-transverse-electric (TE) or quasi-transverse-magnetic (TM) mode (electric field parallel or perpendicular to the substrate plane) from an amplified spontaneous emission light source. First, we measured the polarization controller IL as

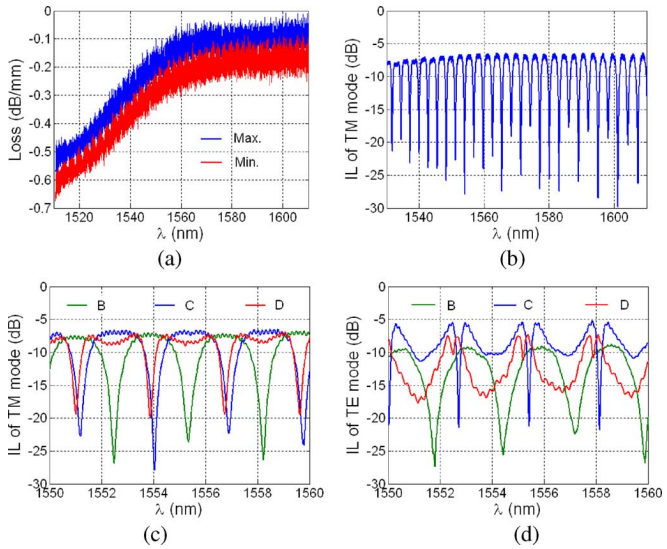

Fig. 4. Transmission spectra: (a) Propagation loss for unit waveguide length; (b) panorama view of the TM mode response spectrum; (c) spectra of the TM modes, corresponding to the three coupling situations, (d) spectra of the TE modes, corresponding to the three coupling situations.

the reference. Then, we deducted the polarization controller IL from the following measurements.

IV. Results and Discussion

The unit length propagation loss of the waveguide is shown in Fig. 4(a). It includes the maximum (blue) and minimum (red) losses per unit millimeter. The transmission spectrum of the waveguide is shown to be flat when the wavelength is greater than 1560 nm (maximum: ~ -0.1 dB/mm; minimum: ~ -0.2 dB/mm) while it has higher loss for a shorter wavelength. PDL is $\sim$0.1 dB for the millimeter unit.

Fig. 4(b)–(d) are spectra scanned by an optical spectrum analyzer (OSA). In Fig. 4(b), the scanned range of wavelength is from 1530 to 1610 nm with a scanning step of 0.05 nm. Fig. 4(b) is the spectrum with TM polarization. An expanded view is shown as a blue curve in Fig. 4(c), where the spectrum ranges from 1550 to 1560 nm. The spectrum shows flat-top. The -1-dB passband width is $\sim$57% of the channel spacing. For comparison, the other two situations are also demonstrated in Fig. 4(c) and (d). The three curves are corresponding to Fig. 3(B), (C), and (D), respectively. The green curve (curve B) in Fig. 4(c) is a little hunch, and the red curve (curve D) is a little concave. Both curves are compatible with Fig. 2(c). There are slight fluctuations in the curves, caused by the reflections of the input and output surfaces.

Although PDL of the waveguide is small, the whole device still shows discernable polarization dependence. The transmission of TE mode is also shown in Fig. 4(d). The coupling efficient is polarization-dependent. From the simulation of a simple model—directional coupler model—we verified that the self-coupling coefficient of the TE mode is larger than that of the TM one. The varied coupling regions offer different light phase shifts. This will result in a wavelength shift in the spectrum as can be seen from curves (B), (C), and (D) in Fig. 4(c) and (d). Moreover, curve (B) (green line) has a greater wavelength shift because the cross light has half that of the π difference between those of the situations of the connected and the separated gaps.

V. Conclusion

A novel double-ring resonator comb filter structure with flat-top response has been proposed. We analyzed its function theoretically, and fabricated the structure on SiN. The measured results showed a flat-top response profile for the TM mode. The measured channel isolation was $\sim$15 dB, the FSR was $\sim$3 nm. The device was compact; a footprint of $\sim 450\ \mu\text{m} \times 250\ \mu\text{m}$ was achieved. Since the structure of the double-ring resonator comb filter is a special MZI structure, we can modulate the two arms with thermo-optical or plasmon dispersion effects. Thus, the structure can be made as comb filter-based modulator or switch. Furthermore, combining with gain materials, building a multiwavelength laser is feasible.

References

[1] X. J. Gu, "Wavelength-division multiplexing isolation fiber filter and light source using cascaded long-period fiber gratings," *Opt. Lett.*, vol. 23, pp. 509–510, 1998.

[2] Y. T. Dai, X. F. Chen, X. M. Xu, C. C. Fan, and S. Z. Xie, "High channel count comb filter based on chirped sampled fiber Bragg grating and phase shift," *IEEE Photon. Technol. Lett.*, vol. 17, no. 5, pp. 1040–1042, May 2005.

[3] Y. W. Lee, H. T. Kim, J. Jung, and B. H. Lee, "Wavelength-switchable flat-top fiber comb filter based on a Solc type birefringence combination," *Opt. Express*, vol. 13, pp. 1040–1048, Feb. 2005.

[4] X. W. Shu, K. Sugden, and I. Bennion, "Novel multipassband optical filter using all-fiber Michelson–Gires–Tournois structure," *IEEE Photon. Technol. Lett.*, vol. 17, no. 2, pp. 384–386, Feb. 2005.

[5] B. J. Offrein, F. Horst, G. L. Bona, H. W. M. Salemink, R. Germann, and R. Beyeler, "Wavelength tunable 1-from-16 and flat passband 1-from-8 add–drop filters," *IEEE Photon. Technol. Lett.*, vol. 11, no. 11, pp. 1440–1442, Nov. 1999.

[6] K. Jinguji and M. Oguma, "Optical half-band filters," *J. Lightw. Technol.*, vol. 18, no. 2, pp. 252–259, Feb. 2000.

[7] Q. Wu, P. L. Chu, H. P. Chan, and B. P. Pal, "Polymer-based compact comb filter with flat top response," *IEEE Photon. Technol. Lett.*, vol. 17, no. 12, pp. 2619–2621, Dec. 2005.

[8] S. Bidnyk, A. Balakrishnan, A. Delâge, M. Gao, P. A. Krug, P. Muthukumaran, and M. Pearson, "Planar comb filters based on aberration-free elliptical graing facets," *J. Lightw. Technol.*, vol. 23, no. 3, pp. 1239–1243, Mar. 2005.

[9] J. Song, Q. Fang, S. H. Tao, M. B. Yu, G. Q. Lo, and D. L. Kwong, "Proposed silicon wire interleaver structure," *Opt. Express*, vol. 16, no. 11, pp. 7849–7859, May 2008.

[10] J. Song, Q. Fang, S. H. Tao, M. B. Yu, G. Q. Lo, and D. L. Kwong, "Passive ring-assisted Mach–Zehnder interleaver on silicon-on-insulator," *Opt. Express*, vol. 16, no. 12, pp. 8359–8365, Jun. 2008.

[11] K. Wörhoff, C. G. H. Roeloffzen, R. de Ridder, A. Driessen, and P. V. Lambeck, "Design and application of comact and highly tolerant polatization-independent waveguides," *J. Lightw. Technol.*, vol. 25, no. 5, pp. 1276–1283, May 2007.